Influence of phosphate anion adsorption on the kinetics of oxygen electroreduction on low index Pt(*hkl*) single crystals†

Qinggang He,[a] Xiaofang Yang,[b] Wei Chen,‡[c] Sanjeev Mukerjee,*[a] Bruce Koel[b] and Shaowei Chen*[c]

Received 3rd May 2010, Accepted 15th July 2010
DOI: 10.1039/c0cp00433b

The detrimental effects of phosphate anion adsorption on the oxygen reduction reactions (ORR) on low index Pt single crystal electrodes were studied in 0.1 M perchloric acid by using a hanging meniscus rotating disk electrode in the presence of varied concentrations of H_3PO_4. The kinetic current for ORR decreased dramatically on Pt(100), Pt(110), Pt(111), and PtSn(111) even with the addition of a small amount (1 mM) of H_3PO_4 into the perchloric acid solution, most probably due to the adsorption of phosphate anions onto the Pt active sites that impeded the electroreduction of O_2. Remarkably, the extent of decline was found to vary with the specific single crystal surface, following the order of Pt(111) > PtSn(111) > Pt(110) ~ Pt(100). Consistent behaviors were also observed in Tafel analysis and in electrochemical impedance spectroscopic measurements. Within the present experimental context, Pt(110) was found to be the optimal crystal surface for ORR in phosphoric acid fuel cells with the smallest charge transfer resistance, whereas the poisoning effects of phosphate anion adsorption were the most pronounced on Pt(111), most likely because the phosphate anions primarily adsorbed on the 3-fold sites on the Pt(111) faces, as manifested in *in situ* X-ray absorption spectroscopic measurements.

1. Introduction

Phosphoric acid fuel cells (PAFC) have been commercialized successfully and used for stationary applications with a combined heat and power efficiency of about 80%.[1] However, continuous improvements are still imperative if PAFCs are to hold their positions in the market or penetrate into other areas with moving targets in terms of cost and efficiency.[2] Currently, the most favored materials for PAFC cathode catalysts are Pt in high-surface-area forms (*i.e.*, nanosized particles) supported on carbon. Over the years, extensive studies have been carried out for the preparation of ultrasmall Pt particles so as to maximize the surface to volume ratio.[3] Recent improvements in membrane electrode assembly (MEA) technologies have made it possible to achieve ready accessibility to the electrolyte and gaseous phases for all catalyst-containing parts, and a three-phase contact between the electrolyte film, gaseous reactant, and the electronically conducting catalyst support.[4] However, one major factor that limits the performance of PAFCs is the sluggish kinetics of oxygen reduction reactions (ORR) in H_3PO_4, and this is attributed primarily to the poisoning effects of phosphate ion adsorption ($H_2PO_4^-$) on ORR activity. As the adsorption of anions is structure-sensitive, the ORR performance is anticipated to vary sensitively with the surface structure of the catalysts.[5] Furthermore, the adsorption may be reversible (*e.g.*, adsorption of hydroxyl species from water activation) or partially reversible (*e.g.*, adsorption of sulfate, phosphate, halogen, *etc*). The effect of such adsorption on the pathway of ORR, *i.e.*, site blocking or rendering alternative lower energy transition states to be formed, is of great interest in designing the next-generation electrocatalysts with improved performance. At a fundamental level, understanding electrocatalytic pathways on single crystal surfaces provides important insights. However translating these results to experimental observations on highly dispersed nanocluster polycrystalline materials is somewhat difficult especially in the size range below 2 nm, where there is an exponential increase in non-bulk planes such as edge, kink and vertex sites. The wealth of literature however points to improved electrocatalysis for ORR for particle sizes significantly higher than 4–5 nm where bulk planes (100, 111, 110, *etc*.) predominate.[6]

Adsorption of anions such as (bi)sulfate,[7–12] chloride,[5,13,14] and hydroxyl[15,16] on Pt single crystals and Pt nanoparticles in an electrochemical environment has been extensively studied. However, there are only a few reports about phosphate anion adsorption on Pt, possibly because of the polyprotic nature[17] of phosphoric acid that makes the study complicated. Weber *et al.*[18] claimed that the adsorption of phosphate species was

[a] *Department of Chemistry & Chemical Biology, Northeastern University, 360 Huntington Ave, Boston, MA 02115, USA. E-mail: s.mukerjee@neu.edu*
[b] *Department of Chemistry and Center for Advanced Materials and Nanotechnology, Lehigh University, Bethlehem, PA 18015, USA*
[c] *Department of Chemistry and Biochemistry, University of California, 1156 High Street, Santa Cruz, CA 95064, USA. E-mail: schen@chemistry.ucsc.edu*

† Electronic supplementary information (ESI) available: Additional experimental data including RDE voltammograms and *in situ* X-ray absorption spectra of the single crystal electrodes. See DOI: 10.1039/c0cp00433b

‡ Present address: State Key Laboratory of Electroanalytical Chemistry, Changchun Institute of Applied Chemistry, Chinese Academy of Sciences, Changchun 130022, China.

insensitive to the Pt surface geometry with mainly $H_2PO_4^-$ adsorbed in the low potential region and a mix of $H_2PO_4^-$ and HPO_4^{2-} adsorbed in the high potential regime. In contrast, Tanaka *et al.*[19] believed that the phosphate anion adsorption was structure-dependent as manifested by the variation of ORR in H_3PO_4 solutions with electrode structure. It should be noted that there exists considerable differences in the published literature on the exact nature and mode of phosphate adsorption on Pt surfaces. For instance, it has been found that both $H_2PO_4^-$ and HPO_4^{2-} can be adsorbed on the Pt(111) and Pt(100) surfaces. In one study based on *in situ* FTIR measurements, it was argued that the stretching vibrations of the $H_2PO_4^-$ ion occurred through two oxygen atoms with C_{2v} symmetry and those of HPO_4^{2-} ion through three equivalent oxygen atoms with C_{3v} symmetry.[18] Yet in another study, Tanaka *et al.* proposed that the adsorption of phosphate anions occurred *via* three oxygen atoms on the Pt(111) surface in the three-fold sites and only one or two oxygen atoms were involved in the adsorption on Pt(100) and Pt(110) surfaces.[19] In the context of these prior reports it is important to note that in the concentration range of 1 to 100 mM the predominant species is expected to be dihydrogen phosphate anion ($H_2PO_4^-$) (concentration six orders of magnitude higher than that of HPO_4^{2-}) when considering the corresponding dissociation constants (5 orders of magnitude difference) at room temperature at pH 0 to 1.

A few studies have been reported in the literature about the kinetics of ORR on single crystal Pt surfaces in H_3PO_4. Tanaka *et al.*[19] demonstrated a four-electron process for ORR with first-order kinetics on three low-index Pt single crystals in 0.1 M H_3PO_4 and concentrated 85% H_3PO_4. An order of Pt(110) > Pt(100) > Pt(111) in terms of catalytic activity towards ORR was provided in their study. Kadiri *et al.*[8] found that the ORR activity varied on different Pt single crystals with the sequence of Pt(110) > Pt(100) > Pt(111) in 1 M H_3PO_4. They believed that ORR was orientation and structure-sensitive in H_3PO_4 solution and anion adsorption might change according to the surface structure of the single crystal electrodes. However, insufficient proofs have been given in the above literature to draw the conclusion that the order of catalytic activity noticed is purely caused by structure-dependent phosphate anions adsorption given the fact that ORR is a structural dependence reaction itself on Pt surface.[12,13,20–22]

Strategically, deterioration of ORR kinetic current (ΔI_k) can be assessed by conducting ORR measurements in the presence and absence of H_3PO_4 on a Pt single crystal with unique surface orientation. Comparison of ΔI_k on different Pt single crystals will provide us with the information on how the specific adsorption interferes with ORR on Pt with various surface morphologies, where only the structure-dependent adsorption of the phosphate anion plays the contributing role.

Within this context, the goal of this work is to further our understanding of the effects of phosphate adsorption on oxygen reduction by using single crystal Pt electrodes in 0.1 M $HClO_4$ with the addition of different amounts of H_3PO_4 (1 to 100 mM). Incremental dosing of H_3PO_4 was (a) to detect any changes in anion adsorption mode and (b) to determine the threshold concentration beyond which no further poisoning effect is observed. A hanging meniscus rotating disk (HMRD) electrode was used to quantitatively determine the kinetic parameters of ORR on three low-index Pt single crystals (Pt(100), Pt(110), and Pt(111)) as well as a surface modified single crystal (PtSn(111)) electrode. The poisoning effects of phosphate adsorption on ORR charge transfer dynamics were then examined by voltammetry and electrochemical impedance spectroscopy (EIS). The choice of well ordered PtSn(111) was aimed at elucidating the effect of (a) alloying from the perspective of a crystal plane with the highest atomic density (111), and (b) Sn being most easily oxidized, its presence in an ordered atomic array in the context of its effect on phosphate anion adsorption (concomitant comparison with Pt(111)). These investigations were aimed at providing pointers in better designs of polycrystalline nanoparticles whose relative population of bulk crystal planes and nature of available sites can be engineered *via* adjustment of particle size and choice of alloying elements. *In situ* X-ray absorption spectroscopy was employed to elucidate the site-specific adsorption of phosphate anions on Pt single crystal surfaces.[14,23–26]

2. Experimental section

2.1 Preparation of single crystals

The preparation and cleaning of the Pt single crystals were performed in a stainless steel ultra-high vacuum (UHV) chamber with a base pressure of 1.0×10^{-10} Torr. This system is equipped with low energy ion scattering (LEIS), high-resolution X-ray photoelectron spectroscopy (XPS), and low energy electron diffraction (LEED). The crystals were cleaned by cycles of Ar^+ sputtering (2.0×10^{-5} Torr, 500 eV) and annealed at 900 K in 5.0×10^{-8} Torr of oxygen. Flushing to 1100 K was required to remove residual oxygen and sharp LEED patterns were obtained to ensure good quality of the single crystal surfaces. The electrodes were typically cooled down in a H_2/Ar atmosphere to lift the reconstruction when the electrodes were still hot. A tin doser was also used to evaporate Sn on Pt(111) to generate a Sn/Pt(111, 2×2) alloy surface, followed by annealing to different temperatures as described by Xu *et al.*[27] LEIS and XPS were also performed to ensure that all surfaces were free of even trace levels of impurities. The cleaned crystals were then transferred from the UHV chamber to an argon gas-filled box. In this box, a working electrode was made by mounting a crystal onto the top of a rotating disc electrode through a spot-welding method. Briefly, a small metal wire was welded onto the low edge of the crystal and side of the rotating disc electrode. This epoxy-free working electrode was very stable during rotation. A hanging meniscus rotating disc technique was used in the electrochemical measurements. The height of the meniscus was carefully controlled to prevent the side of crystals from contacting the solution (lateral wetting).

Because of irreversible adsorption of phosphoric acid on Pt single crystal surfaces which might lead to adsorption-induced surface reconstruction, the Pt surfaces were prepared independently for each electrochemical measurement. Surface cleanliness and LEED patterns were checked before each

experiment. Typically, each electrode was treated three times before being used in electrochemical measurements. The surface areas of these single crystal electrodes were Pt(100), 0.810 cm^2; Pt(110), 0.712 cm^2; Pt(111), 0.568 cm^2; and PtSn(111), 0.502 cm^2.

2.2 Electrochemical measurements

Electrochemical measurements were conducted in a standard three-compartment electrochemical cell at room temperature using a rotating disk electrode (RDE) setup from Pine Instruments connected to an Autolab potentiostat (Ecochemie Inc., Model-PGSTAT 30). All potentials were measured with respect to a sealed hydrogen reference electrode (RHE) made from the same electrolyte used in the ORR experiments. A platinum wire was used as the counter electrode. The electrolytes were prepared with $HClO_4$ (GFS Chemicals) and purified H_3PO_4 (Sigma-Aldrich) using standard procedures described in the literature.[28]

Voltammetric measurements were carried out with Pt(111), Pt(110), Pt(100), and PtSn(111) electrodes in either deoxygenated or oxygen-saturated 0.1 M $HClO_4$ with the addition of different amounts of H_3PO_4 (1 to 100 mM). EIS measurements were conducted at +0.85 V (*vs.* RHE) by using an EG&G PARC Potentiostat/Galvanostat (Model 283) and Frequency Response Detector (Model 1025). The impedance spectra were recorded between 100 kHz and 10 mHz with the amplitude of the ac signal at 5 mV.

3. Results and discussion

3.1 Cyclic voltammetry

Fig. 1 shows the cyclic voltammograms of (a) Pt(100), (b) Pt(110), (c) Pt(111) and (d) PtSn(111) single crystal electrodes in 0.1 M $HClO_4$ with the addition of different amounts of H_3PO_4 (note that at this pH, ~1, the dominant ionization product of H_3PO_4 is $H_2PO_4^-$). It can be seen that before the addition of H_3PO_4 all three electrodes exhibited voltammetric features that were consistent with those reported in the literature,[22,29] indicating well-defined crystalline

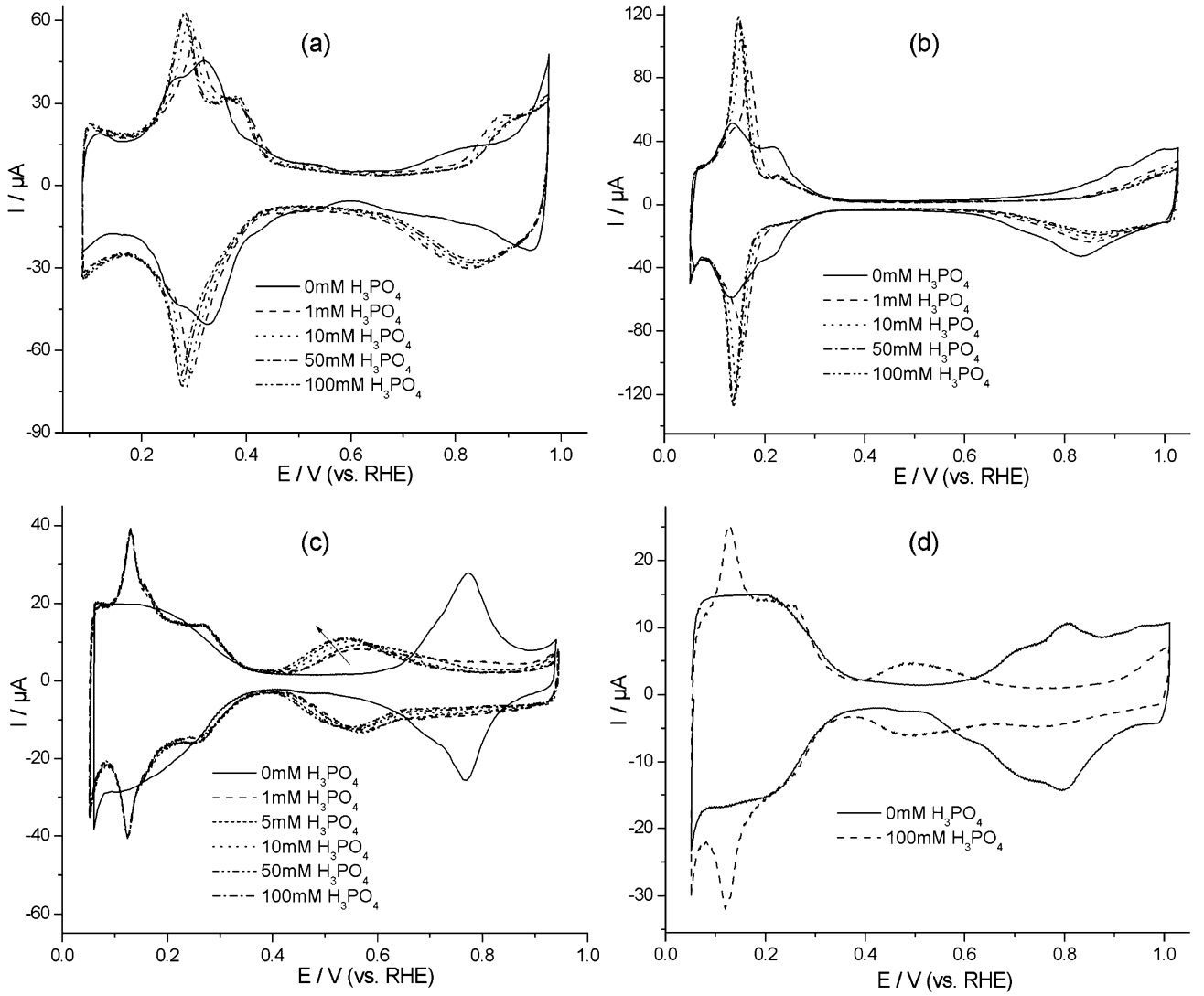

Fig. 1 Cyclic voltammograms of (a) Pt(100), (b) Pt(110), (c) Pt(111) and (d) PtSn(111) electrodes in 0.1 M $HClO_4$ with the addition of various amounts of H_3PO_4 (shown as figure legends). Potential scan rate 50 mV s^{-1}.

surfaces (further confirmed by the corresponding LEED measurements, not shown). Additionally, symmetrical voltammetric peaks appeared in the hydrogen UPD (H_{upd}) region of $E < +0.4$ V.

Upon the addition of H_3PO_4, the (a) Pt(100) and (b) Pt(110) electrodes both exhibited a diminishment of the double layer currents, and the decrease was more pronounced at Pt(100) than at Pt(110). To account for these observations, it should be noted that the onset potential for phosphate anion adsorption on the Pt(100) surface was no less than +0.3 V (*vs.* RHE).[18] Thus, the peaks seen in the H_{upd} region in panel (a) might be attributed to H adsorption on the (100) bi-dimensional sites, and the new anodic peak at *ca.* +0.4 V most likely arose from surface reconstruction induced by the adsorption of phosphate ions.[30] A similar observation was reported with Au(100) that was found to undergo surface reconstruction (1 × 1 ↔ hexagonal) after anion adsorption,[18,30] leading to the appearance of extra positive charges on the electrode surface due to a change of the potential of zero charge (pzc). In contrast, no surface reconstruction was observed at Pt(110) (panel b). Yet, the suppression of the H_{upd} peak at *ca.* +0.23 V and the growth of the one at +0.14 V might be ascribed to the stronger adsorption of phosphate anion at more positive electrode potentials.

The behaviors of the Pt(111) electrode were somewhat different. From panel (c), it can be seen that the voltammetric currents at Pt(111) were virtually invariant in the H_{upd} region with the addition of H_3PO_4, where the anomalous state or butterfly envelope feature[18] remained very well defined and shifted cathodically with increasing concentrations of H_3PO_4. However, there was a pair of new peaks emerging at *ca.* +0.55 V which was attributable to the specific adsorption/desorption of phosphate ions.[19,31] Similar findings were reported in Nikolic's work in the determination of the valence state of phosphate anions adsorbed on Pt(111).[31] Notably, an appreciable change was seen even after the addition of 1 mM H_3PO_4 into the electrolyte solution. Further addition of H_3PO_4 caused only slight changes of the voltammetric currents and adsorption equilibrium was reached after the addition of 50 mM H_3PO_4. The adsorption of phosphate anions occurred after the desorption of H and ceased at the onset potential of OH adsorption. Notably, the inhibition to water activation[32] and Pt oxide formation[18,33] (positive shift of onset potential) on Pt(111) due to the adsorption of phosphate anions appears to be more prominent than that on Pt(100) and Pt(110), which will be discussed in more detail in the next section of oxygen reduction.

The differences observed in the voltammetric responses for the different bulk crystal planes mentioned above in the presence of phosphate anions might be further understood by considering the different surface structures of the Pt single crystals. As an FCC crystal, Pt exposes a closed packed hexagon in the (111) face, where adsorption might occur at the atop, bridge, and hollow sites, whereas atoms on the (110) face exhibit an up and down arrangement, and the ideal (110) face is not energetically favorable, which may be reconstructed to form a (2 × 1) structure with missing rows in the (110) direction. This reconstructed surface actually exposes two kinds of (111) planes, which are perpendicular to each other with only two rows of atoms exposed on the (111) surface. The space hindering effect prevents phosphate anions from adsorbing on these two (111) planes simultaneously. Atoms in the (100) surface, however, display a square arrangement, which is not energetically favorable either. Surface reconstruction of the ideal (100) surface forms a quasi-hexagonal packing structure,[34–36] which might be removed by the adsorption of small molecules such as NO, CO, *etc.*[37]

In order to investigate phosphate anion adsorption on alloyed Pt single crystals, we also prepared a Pt_3Sn(111, 2 × 2) surface alloy by evaporating Sn onto Pt(111) in UHV, followed by thermal annealing at 1000 K to obtain a clear and sharp (2 × 2) LEED pattern. The voltammetric features of PtSn(111) in 0.1 M $HClO_4$ and 0.1 M $HClO_4$ + 100 mM H_3PO_4 (Fig. 1(d)) were very similar to those depicted in Fig. 1(c) for Pt(111).

In summary, based on the voltammetric studies, it can be seen that the adsorption of phosphate anions depends highly on the facets and orientation of the Pt single crystal electrodes, and the adsorption occurs most saliently on Pt(111), as manifested in *in situ* X-ray absorption spectroscopy measurements (Figs. S1 and S2, ESI†), which is anticipated to lead to severe inhibition of water activation and oxide species formation, as discussed in further detail below.

3.2 ORR study

To minimize the complication arising from the polyprotic nature of H_3PO_4,[17] we opted to maintain a constant solution pH while keeping the concentration and diffusion coefficient of O_2 constant for ORR measurements.[19] Fig. 2 shows the RDE voltammograms of ORR at Pt(100), Pt(110), Pt(111), and PtSn(111) single crystal electrodes in 0.1 M $HClO_4$ (pH ≈ 1) at 900 rpm. The ORR curves on these electrodes at other rotation rates can be seen in Fig. S3 (ESI†). Three regions may be identified, namely, the kinetics controlled region (> +0.9 V), mixed diffusion-kinetic limitation region (+0.7 V to +0.9 V) and a diffusion-controlled region

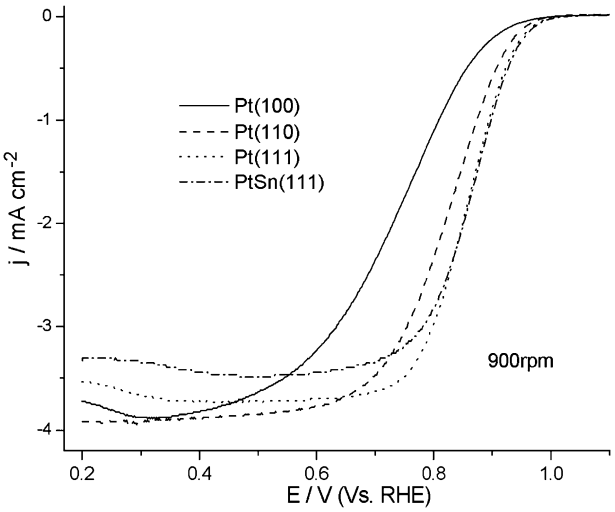

Fig. 2 RDE voltammograms for the Pt(100), Pt(110), Pt(111), and PtSn(111) electrodes in O_2 saturated 0.1 M $HClO_4$ at 900 rpm. The current density was calculated by normalizing the voltammetric current to the geometrical area of the electrode. DC ramp 20 mV s^{-1}.

(< +0.7 V). However, the diffusion-controlled region on Pt(100) is not well defined, especially at high rotation rates, which may be accounted for by (i) the surface tension at the Pt(100) surface that renders it difficult for O_2 to transport from the solution to the electrode surface through the thin film of electrolyte,[19] and (ii) traces of Cl^- and NO_3^- in the solution that are prone to adsorb on Pt(100) and hence affect ORR.[12,22,38] In addition, the small decrease of limiting currents at $E < +0.3$ V with (a) Pt(100) and (c) Pt(111) might be attributable to H adsorption on the Pt surface active sites. Such a decrease did not happen on (b) Pt(110). Additionally, of note is that the shape of the current–potential curves on (c) Pt(111) and (d) PtSn(111) is very similar, again, signifying a Pt-rich surface on the PtSn(111) electrode.

The ORR current density (j) can be expressed by the Koutecky–Levich equation,[39]

$$\frac{1}{j} = \frac{1}{j_k} + \frac{1}{j_L} \quad (1)$$

where j_k is the kinetic current density, j_L is the diffusion limiting current density. Due to the hydrodynamic behaviors of the hanging meniscus rotating disk system,[12,21,40] the diffusion limiting current density (j_L) has to be described by using a modified Levich equation,[12,22]

$$j_d = 0.620nFD^{\frac{2}{3}}C_O\nu^{-\frac{1}{6}}\omega^{\frac{1}{2}}[1 - 2KR_0^{-1}(\nu/\omega)^{\frac{1}{2}}] \quad (2)$$

where n is the number of electron transfer, ω is the rotation rate, F is the Faraday constant, D is the diffusion coefficient of O_2 in 0.1 M $HClO_4$ solution, ν is the kinematic viscosity, C_O is the concentration of molecular oxygen, R_0 is the geometric radius of the electrode, and K is a constant related to the meniscus height.

The plots of j_L *vs.* $\omega^{\frac{1}{2}}$ are depicted in Fig. 3 based on data collected from Fig. S3 (ESI†), which show a linear plot and negative intercept for all electrodes, as anticipated from eqn (2). The experimental slopes are similar to the theoretical Levich plot with $n = 4$ (Table 1), indicating that the ORR followed the 4-electron reduction pathway to water on all the Pt single crystal electrodes. The negative intercepts indicate that the lateral wetting effect was minimal.[12]

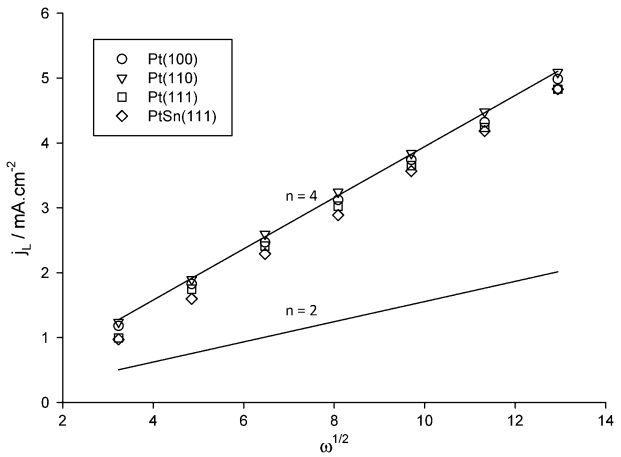

Fig. 3 Plot of limiting current density (j_L) *vs.* square root of rotation rate ($\omega^{\frac{1}{2}}$) for O_2 reduction at Pt(100), Pt(110), Pt(111), and PtSn(111) electrodes in O_2-saturated 0.1 M $HClO_4$. Symbols are experimental data acquired from Fig. S3 (ESI†), and solid lines are simulations with $n = 2$ and $n = 4$ by the Levich equation.

Further analysis based on eqn (1) and (2) shows that the plots of j^{-1} *vs.* j_L^{-1} are all linear and parallel at different potentials (Fig. 4), demonstrating that the kinetics of ORR on these single crystal electrodes is first order with O_2.[22] The intercept of each plot reflects the value of j_k at a specific electrode potential, which may be correlated with the reaction rate constant (k_E) by eqn (4).[12,22,41]

$$j_k = nFk_EC_O \quad (3)$$

The k_E values of the varied single crystal electrodes in different acid systems are summarized in Table 1, where one can see that on all these Pt single crystals, k_E decreases with increasing H_3PO_4 concentration, indicating that the ORR reaction becomes more and more sluggish due to the adsorption of phosphate anions.

The effects of phosphate anions adsorption on ORR on different crystallographic planes are further manifested in Fig. 5 and 6. Both anodic and cathodic ORR curves on Pt(111) in 0.1 M $HClO_4$ and 0.1 M $HClO_4$ + 50 mM H_3PO_4 are shown in Fig. 5 (those for Pt(100) and Pt(110) were included in Fig. S4 (ESI†)). Two conclusions can be drawn from these data: (a) in the presence of H_3PO_4 in the electrolyte solution, substantial overpotentials appeared for ORR. (b) It has been well-known that the *hysteresis* between cathodic scan and anodic scan on ORR curves on Pt electrodes is due to the formation of platinum oxide.[42,43] As a result, phosphates do not compete with oxides during adsorption since only a slight change is observed in hysteresis in the presence of phosphate anions. Fig. 6 depicts the RDE voltammograms at the four electrodes in oxygen-saturated 0.1 M $HClO_4$ with the addition of various amounts of H_3PO_4. It can be seen that in all cases, the half-wave potentials ($E_{\frac{1}{2}}$)[22] exhibited an apparent cathodic shift with increasing concentration of H_3PO_4, and the shift varied with the specific crystalline structure of the electrode. For instance, at 100 mM H_3PO_4, the shift of $E_{\frac{1}{2}}$ is 141 mV at Pt(111) (panel c), 99 mV at Pt(100) (panel a), 95 mV at Pt(110) (panel b), and 102 mV at PtSn(111) (panel d). That is, the poisoning effects of phosphate adsorption on the electrocatalytic reduction of oxygen decrease in the order of Pt(111) > PtSn (111) > Pt(100) > Pt(110). This order is also manifested in Fig. 7 which compares the kinetic current density (j_k) at +0.85 V of these four electrodes in the absence and presence of 100 mM H_3PO_4. It can be seen that in all cases, the addition of H_3PO_4 led to substantial diminishment of the kinetic current density. For instance, at Pt(100) electrode, the kinetic current decreased by about 72%; at Pt(100), 76%; at Pt(111), 88%; and at PtSn(111), 83%.

Consistent behaviors were observed in Tafel plots. Fig. 8 depicts the mass-transport corrected Tafel plots of the four single crystal electrodes in 0.1 M $HClO_4$ and 0.1 M $HClO_4$ + 100 mM H_3PO_4, where two slopes may be identified at low and high current density (Table 1). A similar response was also observed for ORR on single crystal and polycrystalline Pt electrodes.[33,44,45] The difference in Tafel slopes observed in

Table 1 Kinetic parameters for ORR on Pt(100), Pt(110), Pt(111) and PtSn(111) single crystals electrodes in 0.1 M $HClO_4$ with the addition of different amounts of H_3PO_4

	H_3PO_4 concentration/mM	n	$E_{\frac{1}{2}}$/V	Tafel slopes[a] at 900 rpm/mV per decade	Rate constant k (10^{-2} cm s^{-1}) at +0.7 V	j_K at +0.85 V, 900 rpm/mA cm^{-2}
Pt(100)	0	3.96	0.736	62.9, 122.3 (Δ = 59.4)	2.01	0.82
	1	4.0	0.698	62.4, 122.0 (Δ = 59.6)	1.02	0.52
	10	3.99	0.673	60.6, 121.3 (Δ = 60.7)	0.78	0.38
	50	3.95	0.642	60.1, 117.5 (Δ = 57.4)	0.70	0.29
	100	3.88	0.637	59.8, 115.2 (Δ = 55.4)	0.50	0.23
Pt(110)	0	4.0	0.822	63.3, 120.5 (Δ = 57.2)	5.60	2.23
	1	3.98	0.779	69.1, 121.2 (Δ = 52.1)	4.18	1.11
	10	4.0	0.752	70.3, 124.0 (Δ = 53.7)	2.16	0.78
	50	3.87	0.728	73.5, 124.3 (Δ = 50.8)	1.62	0.58
	100	3.90	0.720	73.9, 124.9 (Δ = 51)	1.39	0.54
Pt(111)	0	4.0	0.852	64.4, 113.7 (Δ = 49.3)	10.46	3.73
	1	4.0	0.759	72.5, 114.9 (Δ = 42.4)	2.69	0.62
	10	3.98	0.735	77.3, 115.4 (Δ = 38.1)	1.79	0.51
	50	3.94	0.714	80.1, 116.0 (Δ = 35.9)	1.33	0.45
	100	3.88	0.709	80.6, 116.9 (Δ = 36.3)	1.27	0.43
PtSn(111)	0	4.0	0.855	64.5, 111.1 (Δ = 46.6)	8.71	3.74
	1	3.95	0.783	67.8, 111.8 (Δ = 44)	4.19	1.05
	10	4.0	0.760	71.5, 112.7 (Δ = 41.2)	3.14	0.82
	50	3.96	0.754	73.0, 113.1 (Δ = 40.1)	2.35	0.69
	100	3.89	0.753	73.4, 113.4 (Δ = 40)	1.78	0.63

[a] The Tafel slopes at low and high current density are separated by a comma, and Δ denotes the difference between these two slopes.

0.1 M $HClO_4$ can be used to quantify the effect of oxide formation without the interference of anions in the electrolyte since perchloric acid is believed to show minimal poisoning to Pt electrodes.[8,12,22] As a consequence, two typical Tafel slopes of 60 mV per decade and 120 mV per decade can be explained by the fact that the Pt electrode surface is covered by oxides in the low overpotential region and oxide free in the high overpotential region.[12,19,46] Interestingly the transition potentials between the 60 and 120 mV per decade slopes remained virtually invariant at *ca.* +0.90 V for the four single-crystal electrodes both in the absence and presence of H_3PO_4, suggesting that the rate-determining step in ORR was not affected by the adsorption of phosphate anions.[47]

Furthermore, in order to understand the effect of $H_2PO_4^-$ adsorption, it is important to deconvolute it from the concomitant poisoning effect of oxides. If we define Δ as the difference between the Tafel slopes at high (t_h) and low (t_l) current density, *i.e.*, $\Delta = t_h - t_l$, then the difference in 0.1 M $HClO_4$ (Δ_0) and in 0.1 M $HClO_4$ + 100 mM H_3PO_4 (Δ_{100}) can be correlated to the effects of oxides formation and oxides formation plus $H_2PO_4^-$ adsorption, respectively. Therefore, the effect of $H_2PO_4^-$ adsorption (Φ) may be quantified by

$$\Phi = \Delta_0/\Delta_{100} \quad (4)$$

From Table 1, it can be seen that Φ decreases in the order of $\Phi_{Pt(111)}$ (1.36) > $\Phi_{PtSn(111)}$ (1.17) > $\Phi_{Pt(110)}$ (1.12) > $\Phi_{Pt(100)}$ (1.07). The sequence is in line with the trend of catalytic activity drop-off from 0.1 M $HClO_4$ to the solution containing 100 mM H_3PO_4 for ORR on different Pt single crystals shown in Fig. 7.

Whereas it did not appear to affect the ORR reaction pathway (*vide ante*), the adsorption of phosphate anions apparently hindered the oxide species formation and/or O_2 adsorption on Pt and thus impeded the ORR activity, as reflected by the observed variation of the Tafel slopes (Table 1).[33,44,45,48] Notably, the affinity of phosphate anions to the Pt surface varies with the surface crystalline structure, where stronger adsorption resulted in more significant

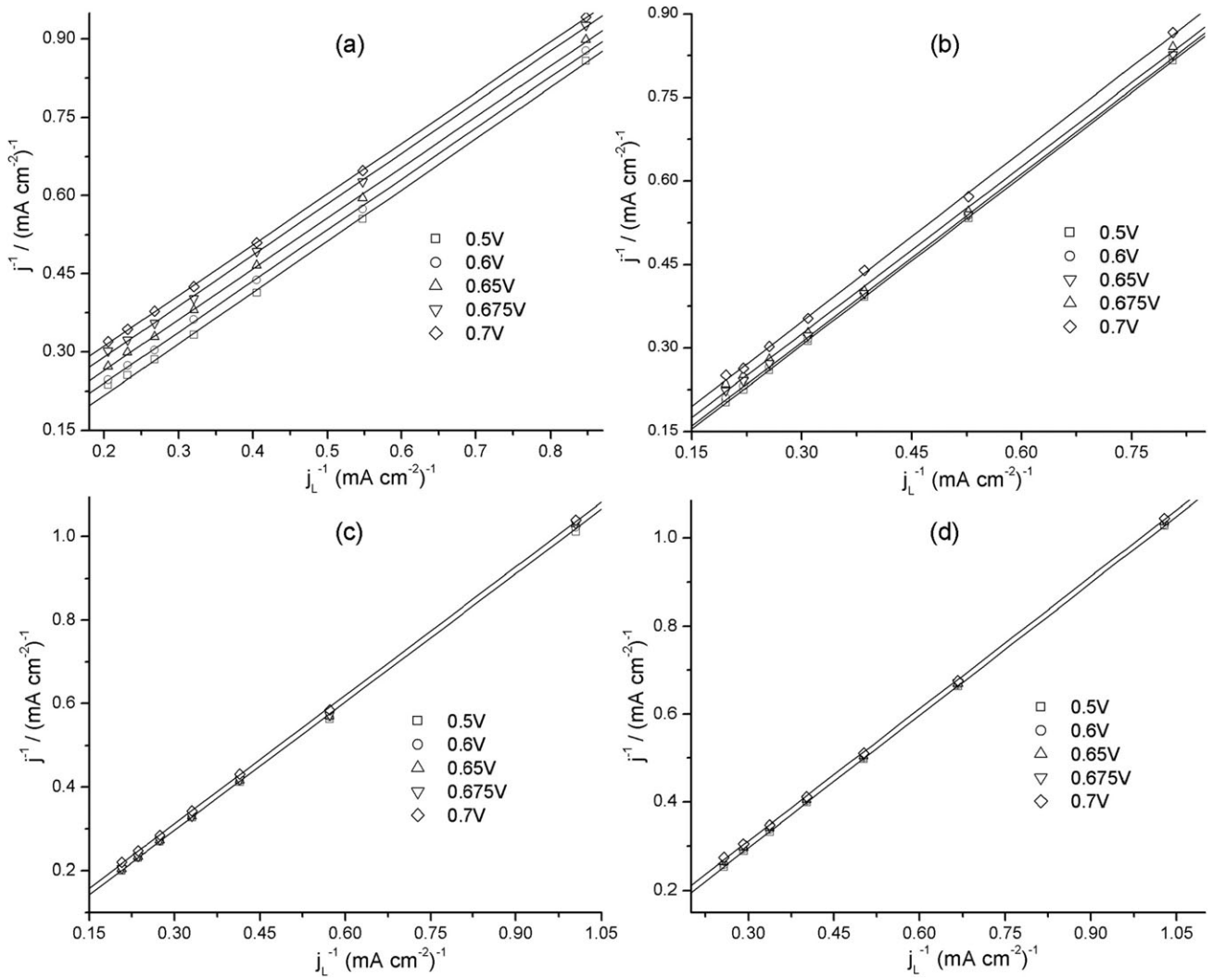

Fig. 4 Plot of j^{-1} *vs.* $j_L{}^{-1}$ for O_2 reduction at (a) Pt(100), (b) Pt(110), (c) Pt(111), and (d) PtSn(111) in O_2-saturated 0.1 M $HClO_4$. Symbols are experimental data acquired from Fig. 3 at different electrode potentials, and lines are linear regressions.

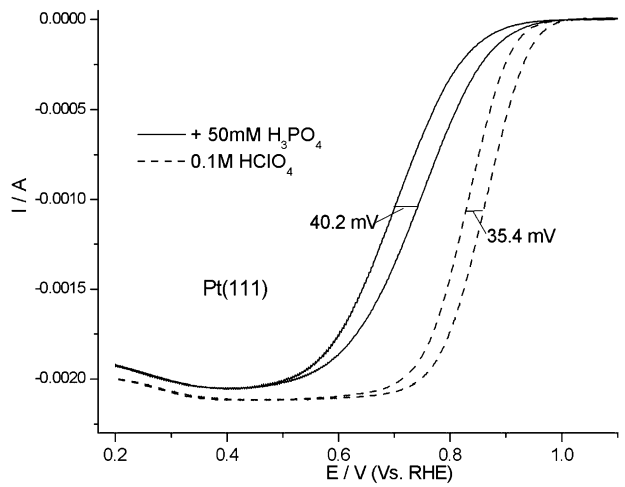

Fig. 5 RDE voltammograms of ORR at Pt(111) electrode in oxygen-saturated 0.1 M $HClO_4$ and 0.1 M $HClO_4$ + 50 mM H_3PO_4. Rotation rate 900 rpm. DC potential ramp 20 mV s^{-1}.

poisoning effects on ORR performance. In the voltammetric studies (Section 3.1), it was found that the adsorption of phosphate anions on Pt(111) was the most pronounced among the four single-crystal electrodes, probably because of the preferred adsorption of phosphate anions on the 3-fold sites as manifested in *in situ* X-ray absorption measurements (Fig. S1 and S2, ESI†). Whereas the adsorption on Pt(110) and Pt(100) was the weakest and yet comparable to each other, an observation consistent with the results from Tafel analyses. Similar observations were reported by Tanaka *et al.*[19] and Kadiri *et al.*[8]

Another interesting observation is that PtSn(111), which was rich with steps and defects, appeared to exhibit enhanced resistance against phosphate poisoning as compared to Pt(111). Although the exact reason remains unclear at this point, a reasonable analogy may be made with Kuzume *et al.*'s study of ORR on stepped Pt surfaces,[21] which showed that the $E_{\frac{1}{2}}$ value for ORR on Pt[n(111) × (111)] surfaces decreased as the step density decreased in sulfuric acid solutions.

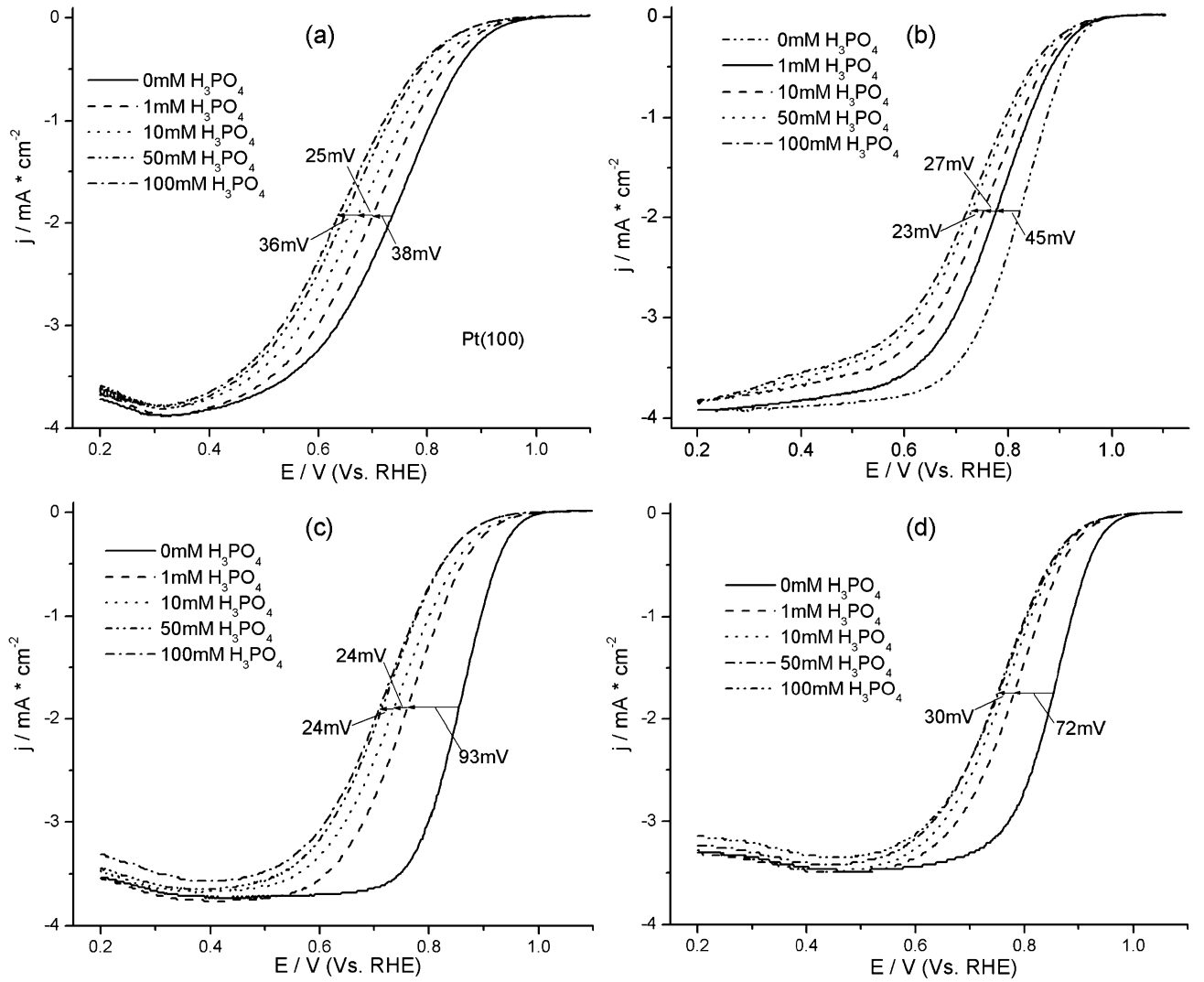

Fig. 6 RDE voltammograms of ORR at (a) Pt(100), (b) Pt(110), (c) Pt(111), and (d) PtSn(111) electrodes in oxygen-saturated 0.1 M $HClO_4$ with the addition of various amounts of H_3PO_4. Current density was based on normalization of voltammetric current to the geometrical area of the electrode. Rotation rate 900 rpm. DC potential ramp 20 mV s^{-1}.

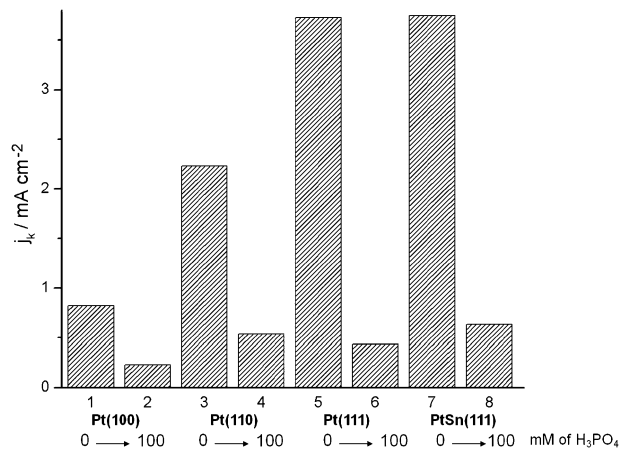

Fig. 7 Kinetic current density of ORR at +0.85 V at Pt(100), Pt(110), Pt(111), and PtSn(111) single crystal electrodes in 0.1 M $HClO_4$ with and without 100 mM H_3PO_4. Data were obtained from Fig. 8.

Note that the Pt[n(111) × (111)] surface is equivalent to Pt[(n − 1)(111) × (110)] where (111) terraces are separated by monatomic (110) steps. With increasing concentration of the (110) steps, the adsorption of (bi)sulfate anions on the (111) terraces was hindered, because the adsorption of (bi)sulfate anions on stepped surfaces gave rise to disordered adlayers, which were less stable than the bi-dimensionally ordered adlayers formed by the adsorption of (bi)sulfate anions on (111) terraces.[8,21] The fact that the geometry[49–51] and properties of adsorption of $H_2PO_4^-$ and HPO_4^{2-} anions on Pt surfaces[52–55] are similar to those of HSO_4^- and SO_4^{2-} makes this analogy reasonable.

3.3 EIS study

Electrochemical impedance spectroscopy (EIS) is a sensitive and powerful technique to study the kinetics of electron-transfer processes. In recent years, EIS has been widely used in fuel cells to study the kinetics of electrode reactions on both

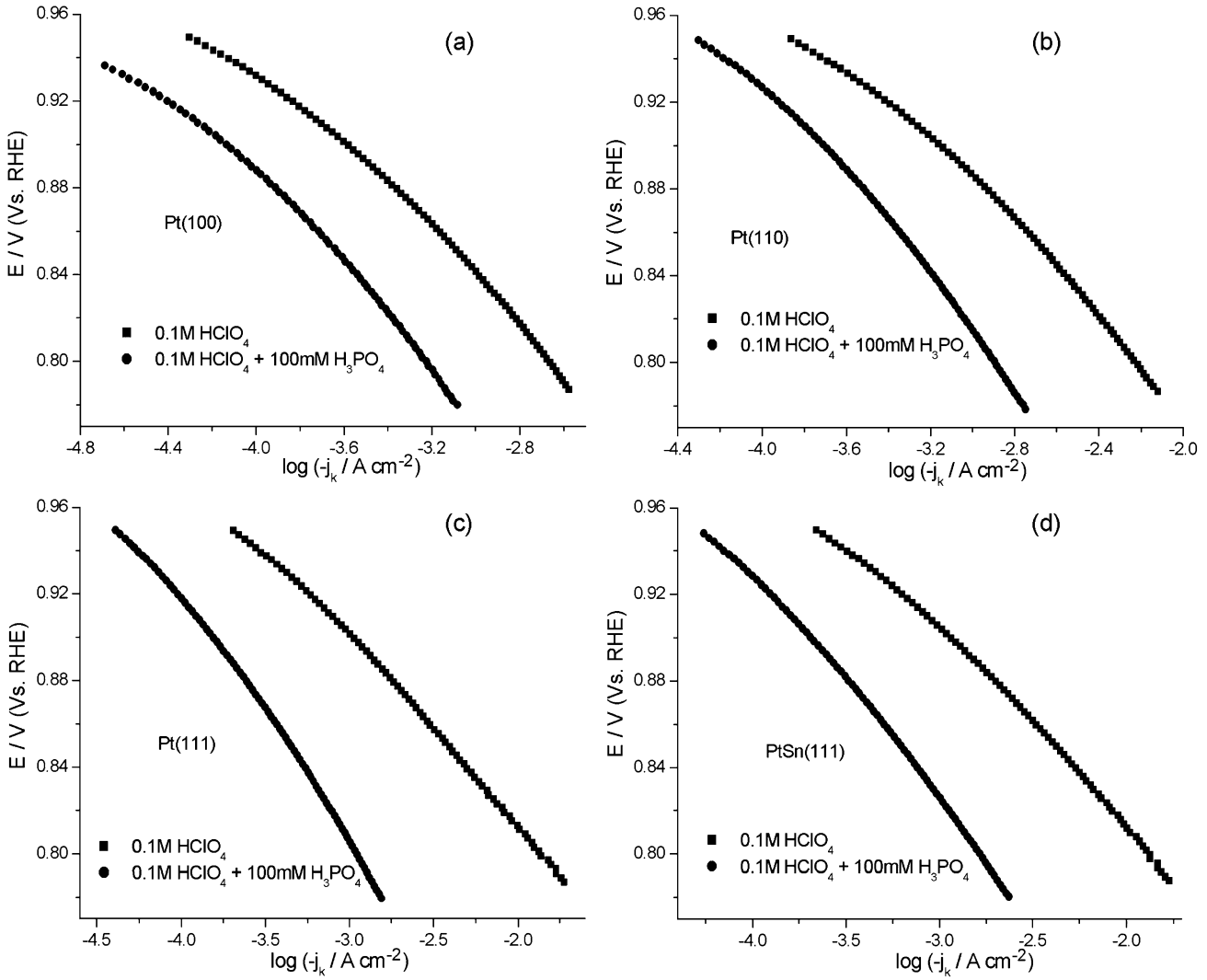

Fig. 8 Mass-transport corrected Tafel plots of ORR at the (a) Pt(100), (b) Pt(110), (c) Pt(111) and (d) PtSn(111) single crystal electrodes in 0.1 M $HClO_4$ and 0.1 M $HClO_4$ + 100 mM H_3PO_4.

the anode[56–58] and the cathode.[59–61] Here, the kinetics of the ORR on the four platinum single crystals as a function of H_3PO_4 concentration is examined by EIS. Fig. 9 shows the Nyquist complex-plane impedance spectra of ORR at +0.85 V (*vs.* RHE) with the four electrodes in O_2 saturated 0.1 M $HClO_4$ in the presence of different concentrations of H_3PO_4 (shown as figure legends). It can be seen that on all the single crystal surfaces under study, the EIS spectra exhibit a well-defined semicircle. Usually for ORR on electrodes with highly rough surfaces (such as those modified with Nafion films and metal nanostructured surfaces), there are two pronounced arcs corresponding to the charge transfer process at high frequencies and the mass transfer process at low frequencies.[62–64] In the present study, the appearance of a single impedance arc suggests that the electrode process under the current experimental conditions is dominated by the interfacial kinetics of the ORR process.

It should be noted that the lower intercept of the impedance arc on the *x*-axis represents the total ohmic resistance of the system, and the diameter of the kinetic arc represents the charge transfer resistance of ORR on the electrode surface. It can be seen clearly that for each electrode in Fig. 9, the diameter of the arcs increases with the increase of H_3PO_4 concentration in the electrolyte. This result indicates that the electrocatalytic activity for ORR decreased by phosphate adsorption on the Pt single crystal surface. Specifically, phosphate anions acted as poisonous species by occupying the active sites on the Pt surface and hence impeded the adsorption of O_2 molecules. Furthermore, one can see that the effect of H_3PO_4 adsorption on the electrocatalytic activity for ORR is strongly dependent on the Pt single crystal surface structures. For example, in O_2-saturated 0.1 M $HClO_4$, the diameter of the impedance arc at Pt(111) is much smaller than that with Pt(100) or Pt(110).

Further insights on the electron-transfer dynamics were obtained by quantitative analysis of the Nyquist impedance spectra, using the equivalent circuit shown in Fig. 10 inset to fit the impedance data.[61] Here, R_S represents the solution (uncompensated) resistance, C_{DL} and R_{CT} are the double layer capacitance and charge transfer resistance, respectively.

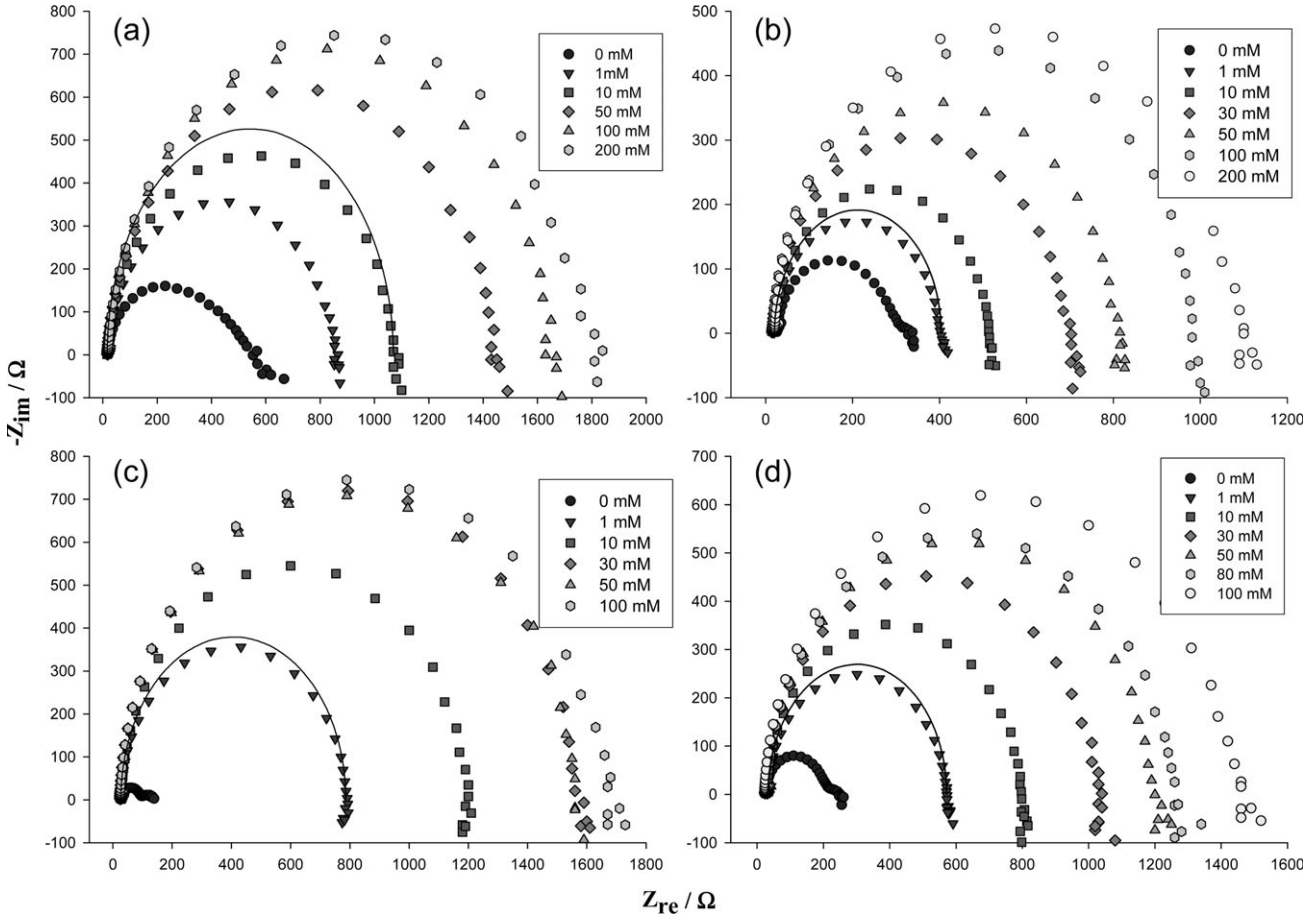

Fig. 9 Complex-plane (Nyquist) impedance plots of ORR at +0.85 V (*vs.* RHE) on (a) Pt(100), (b) Pt(110), (c) Pt(111), and (d) PtSn(111) electrodes in 0.1 M $HClO_4$ with different concentrations of H_3PO_4 (shown as figure legends). Solid lines are representative simulations based on the equivalent circuits shown in Fig. 10 inset.

Representative fits for the four electrodes were shown in each of the Nyquist plots in Fig. 9 (solid lines). It can be seen that all fits are excellent. From the fitting, the variation of the charge transfer resistance (R_{CT}) with the concentration of H_3PO_4 was shown in Fig. 10. It can be seen that on all electrodes R_{CT} increases very quickly with increasing H_3PO_4 concentration and at concentrations greater than *ca.* 50 mM the R_{CT} remains virtually invariant, suggesting that saturated adsorption of phosphate anions was reached in this concentration range.

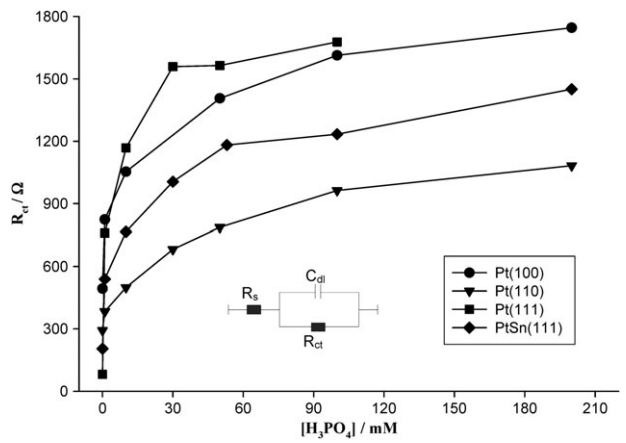

Fig. 10 Charge-transfer resistance (R_{CT}) of ORR as a function of H_3PO_4 concentration in 0.1 M $HClO_4$ at different platinum single crystal electrodes. Data are obtained by curve fitting of the impedance spectra (manifested in Fig. 9) by the equivalent circuit shown in figure inset.

However, the phosphate poisoning effect for ORR on the four Pt electrode surface was drastically different. In the electrolyte without H_3PO_4 (0 mM), R_{CT} on Pt(111), PtSn(111), Pt(110), and Pt(100) is 81.3 Ω, 204.6 Ω, 292.5 Ω, and 493.7 Ω, respectively. With the introduction of H_3PO_4 into the electrolyte solution, R_{CT} increases rather substantially. For instance, at 100 mM H_3PO_4, R_{CT} increases to 1677.4 Ω for Pt(111), 1233.9 Ω for PtSn(111), 963.3 Ω for Pt(110), and 1545.7 Ω for Pt(100). That is, the degree of H_3PO_4 poisoning, reflected by the increase of R_{CT}, decreases in the order of Pt(111) > Pt(100) > PtSn(111) > Pt(110), indicating that Pt(111) is the least active for ORR electrocatalysis in PAFC whereas Pt(110) represents the optimal crystalline surface among the four electrodes. This is consistent with the results based on voltammetric and Tafel analyses (*vide ante*), although the exact sequence of Pt(100) and PtSn(111) is somewhat different.

4. Conclusions

The effects of the adsorption of phosphate anions on the kinetics of ORR on Pt single crystal electrodes were examined by cyclic voltammetry and electrochemical impedance spectroscopy. The ORR kinetics was found to exhibit first-order dependence on the diffusing reactant (O_2) and to proceed *via* a 4-electron pathway with water as the main product on all Pt single crystal electrodes under study. However, upon the introduction of H_3PO_4 into the electrolyte solution, the electrocatalytic performance of ORR was impeded by the adsorption of phosphate anions onto the surface active sites, which decreased in the order of Pt(111) > PtSn(111) > Pt(100) ~ Pt(110), as reflected in voltammetric and electrochemical impedance measurements. The most pronounced poisoning effect observed at Pt(111) was ascribed to the abundant 3-fold surface sites where adsorption of phosphate anions occurred, as manifested in *in situ* X-ray absorption spectroscopic measurements. Additionally, of note is that PtSn(111) showed enhanced tolerance towards phosphate anion adsorption by virtue of the surface steps and defects, suggesting that surface engineering might be an effective route towards the optimization of ORR electrocatalysts.

Acknowledgements

S.W.C. and W.C. thank the National Science Foundation for partial support of this work (CHE-0804049 and CHE-0832605). S.M. and Q.H. thank the financial assistance from Army Research Office under the auspices of a Multi-University Research Initiative lead by Case Western Reserve University and BASF Fuel Cells (Ludwigshafen, Germany). The authors also thank Dr Badri Shyam and Dr David Ramaker for the *in situ* XAS data analysis.

Notes and references

1 R. K. Shah, *Introduction to Fuel Cells*, in *Recent Trends in Fuel Cell Science and Technology*, ed. S. Basu, Anamaya Publishers, 2007.
2 W. Vielstich, A. Lamm and H. A. Gasteiger, *Handbook of Fuel Cells: Fundamentals, Technology, Applications*, Wiley, 2003.
3 A. S. Aricò, V. Antonucci, N. Giordano, A. K. Shukla, M. K. Ravikumar, A. Roy, S. R. Barman and D. D. Sarma, *J. Power Sources*, 1994, **50**, 295.
4 K. H. Yoon, J. Y. Choi, J. H. Jang, Y. S. Cho and K. H. Jo, *J. Appl. Electrochem.*, 2000, **30**, 121.
5 N. M. Markovic, T. J. Schmidt, V. Stamenkovic and P. N. Ross, *Fuel Cells*, 2001, **1**, 105.
6 S. Mukerjee and J. McBreen, *J. Electroanal. Chem.*, 1998, **448**, 163.
7 N. M. Markovic, H. A. Gasteiger and P. N. Ross, Jr., *J. Phys. Chem.*, 1995, **99**, 3411.
8 F. E. Kadiri, R. Faure and R. Durand, *J. Electroanal. Chem.*, 1991, **301**, 177.
9 T. Iwasita, F. C. Nart, A. Rodes, E. Pastor and M. Weber, *Electrochim. Acta*, 1995, **40**, 53.
10 J. X. Wang, N. M. Markovic and R. R. Adzic, *J. Phys. Chem. B*, 2004, **108**, 4127.
11 A. Kolics and A. Wieckowski, *J. Phys. Chem. B*, 2001, **105**, 2588.
12 J. Perez, H. M. Villullas and E. R. Gonzalez, *J. Electroanal. Chem.*, 1997, **435**, 179.
13 V. Stamenkovic, N. M. Markovic and P. N. Ross, *J. Electroanal. Chem.*, 2001, **500**, 44.
14 T. M. Arruda, B. Shyam, J. M. Ziegelbauer, S. Mukerjee and D. E. Ramaker, *J. Phys. Chem. C*, 2008, **112**, 18087.
15 N. M. Markovic, H. A. Gasteiger and P. N. Ross, Jr., *J. Phys. Chem.*, 1996, **100**, 6715.
16 T. J. Schmidt, V. Stamenkovic, P. N. Ross, Jr. and N. M. Markovic, *Phys. Chem. Chem. Phys.*, 2003, **5**, 400.
17 I. R. Moraes and F. C. Nart, *J. Electroanal. Chem.*, 2004, **563**, 41.
18 M. Weber, I. R. de Moraes, A. J. Motheo and F. C. Nart, *Colloids Surf., A*, 1998, **134**, 103.
19 A. Tanaka, R. Adzic and B. Nikolic, *J. Serb. Chem. Soc.*, 1999, **64**, 695.
20 V. Komanicky, A. Menzel and H. You, *J. Phys. Chem. B*, 2005, **109**, 23550.
21 A. Kuzume, E. Herrero and J. M. Feliu, *J. Electroanal. Chem.*, 2007, **599**, 333.
22 N. M. Markovic, R. R. Adzic, B. D. Cahan and E. B. Yeager, *J. Electroanal. Chem.*, 1994, **377**, 249.
23 J. M. Ziegelbauer, D. Gatewood, A. F. Gulla, M. J. F. Guinel, F. Ernst, D. E. Ramaker and S. Mukerjee, *J. Phys. Chem. C*, 2009, **113**, 6955.
24 J. M. Ziegelbauer, D. Gatewood, A. F. Gulla, D. E. Ramaker and S. Mukerjee, *Electrochem. Solid-State Lett.*, 2006, **9**, A430.
25 J. M. Ziegelbauer, V. S. Murthi, C. O'Laoire, A. F. Gulla and S. Mukerjee, *Electrochim. Acta*, 2008, **53**, 5587.
26 J. M. Ziegelbauer, T. S. Olson, S. Pylypenko, F. Alamgir, C. Jaye, P. Atanassov and S. Mukerjee, *J. Phys. Chem. C*, 2008, **112**, 8839.
27 C. Xu, J. W. Peck and B. E. Koel, *J. Am. Chem. Soc.*, 1993, **115**, 751.
28 J. T. Glass, G. L. Cahen, Jr. and G. E. Stoner, *J. Electrochem. Soc.*, 1989, **136**, 656.
29 V. R. Stamenkovic, B. Fowler, B. S. Mun, G. Wang, P. N. Ross, C. A. Lucas and N. M. Markovic, *Science*, 2007, **315**, 493.
30 F. Silva and A. Martins, *Electrochim. Acta*, 1998, **44**, 919.
31 B. Z. Nikolic and R. R. Adzic, *J. Serb. Chem. Soc.*, 1997, **62**, 515.
32 V. S. Murthi, R. C. Urian and S. Mukerjee, *J. Phys. Chem. B*, 2004, **108**, 11011.
33 N. M. Markovic, R. R. Adzic, B. D. Cahan and E. B. Yeager, *J. Electroanal. Chem.*, 1994, **377**, 249.
34 K. Heinz, E. Lang, K. Strauss and K. Mülle, *Surf. Sci.*, 1982, **120**, L401.
35 G. Ritz, M. Schmid, P. Varga, A. Borg and M. Rønning, *Phys. Rev. B: Condens. Matter*, 1997, **56**, 10518.
36 M. A. Van Hove, R. J. Koestner, P. C. Stair, J. P. Bibérian, L. L. Kesmodel, I. Bartoš and G. A. Somorjai, *Surf. Sci.*, 1981, **103**, 189.
37 K. Wu and M. S. Zei, *Surf. Sci.*, 1998, **415**, 212.
38 N. M. Markovic, N. S. Marinkovic and R. R. Adzic, *J. Electroanal. Chem.*, 1988, **241**, 309.
39 E. Higuchi, H. Uchida and M. Watanabe, *J. Electroanal. Chem.*, 2005, **583**, 69.
40 H. M. Villullas and M. L. Teijelo, *J. Electroanal. Chem.*, 1995, **384**, 25.
41 A. J. Bard and L. R. Faulkner, *Electrochemical Methods*, Wiley, 1980.
42 N. M. Markovic, H. A. Gasteiger and P. N. Ross, *J. Phys. Chem.*, 1996, **100**, 6715–6721.
43 Z. Liu, J. S. Wainright, M. H. Litt and R. F. Savinell, *Electrochim. Acta*, 2006, **51**, 3914.
44 A. Tanaka, R. Adzic and B. Nikolic, *J. Ser. Chem. Soc.*, 1999, **64**, 695.
45 A. Damjanov and M. A. Genshaw, *Electrochim. Acta*, 1970, **15**, 1281.
46 S. Gottesfeld, *Electrocatalysis of oxygen reduction in polymer electrolyte fuel cells: a brief history and a critical examination of present theory and diagnostics*, in **Fuel cell catalysis: a surface science approach**, ed. M. T. M. Koper, Wiley: *Hoboken, N.J.*, 2009.
47 N. M. Markovic, H. A. Gasteiger and P. N. Ross, *J. Phys. Chem.*, 1996, **100**, 6715.
48 M. R. Tarasevich, V. A. Bogdanovskaya, L. N. Kuznetsova, A. D. Modestov, B. N. Efremov, A. E. Chalykh, Y. G. Chirkov, N. A. Kapustina and M. R. Ehrenburg, *J. Appl. Electrochem.*, 2007, **37**, 1503.
49 A. Goel, N. Brennan, N. Brady and P. T. M. Kenny, *Biosens. Bioelectron.*, 2007, **22**, 2047.
50 B. P. Hay, D. A. Dixon, J. C. Bryan and B. A. Moyer, *J. Am. Chem. Soc.*, 2002, **124**, 182.

51 E. A. Kataev, G. V. Kolesnikov, E. K. Myshkovskaya, N. N. Popova, I. G. Tananaev and S. I. Rovny, *Vopr. Radiats. Bezop.*, 2008, 16.
52 T. Pajkossy, L. A. Kibler and D. M. Kolb, *J. Electroanal. Chem.*, 2005, **582**, 69.
53 S. Taguchi and A. Aramata, *J. Electroanal. Chem.*, 1998, **457**, 73.
54 S. Takahashi, A. Aramata, M. Nakamura, K. Hasebe, M. Taniguchi, S. Taguchi and A. Yamagishi, *Surf. Sci.*, 2002, **512**, 37.
55 G. Wu, T. Chen, X. Zong, H. Yan, G. Ma, X. Wang, Q. Xu, D. Wang, Z. Lei and C. Li, *J. Catal.*, 2008, **253**, 225.
56 W. Chen, J. Kim, S. H. Sun and S. W. Chen, *Phys. Chem. Chem. Phys.*, 2006, **8**, 2779.
57 W. Chen, J. M. Kim, L. P. Xu, S. H. Sun and S. W. Chen, *J. Phys. Chem. C*, 2007, **111**, 13452.
58 W. Chen, J. M. Kim, S. H. Sun and S. W. Chen, *Langmuir*, 2007, **23**, 11303.
59 L. Genies, Y. Bultel, R. Faure and R. Durand, *Electrochim. Acta*, 2003, **48**, 3879.
60 R. Makharia, M. F. Mathias and D. R. Baker, *J. Electrochem. Soc.*, 2005, **152**, A970.
61 N. Wagner, *J. Appl. Electrochem.*, 2002, **32**, 859.
62 Z. Xie and S. Holdcroft, *J. Electroanal. Chem.*, 2004, **568**, 247.
63 Y. C. Liu, X. P. Qiu, W. T. Zhu and G. S. Wu, *J. Power Sources*, 2003, **114**, 10.
64 S. Y. Cha and W. M. Lee, *J. Electrochem. Soc.*, 1999, **146**, 4055.